Polarization and structure dependent optical characteristics of the three-arm nanoantenna with C_{3v} symmetry and broken symmetry

Mian Wang (王 勉)[1], Cheng Yin (殷 澄)[2], Youqiao Ma (马佑桥)[3], Jun Zhou (周 骏)[1,*], Hanhua Zhong (钟汉华)[1], and Xianfeng Chen (陈险峰)[2]

[1]*Institute of Photonics, Faculty of Science, Ningbo University, Ningbo 315211, China*
[2]*Department of Physics and Astronomy, Shanghai Jiao Tong University, Shanghai 200240, China*
[3]*Department of Electrical and Computer Engineering, Dalhousie University, Halifax, NS B3J 2X4, Canada*
**Corresponding author: zhoujun@nbu.edu.cn*

Received January 3, 2018; accepted March 1, 2018; posted online April 20, 2018

The optical properties of a three-arm plasmonic nanoantenna with and without broken symmetry were analyzed in detail. For the symmetrical structure, the local electric field can be significantly enhanced and well confined within the feed gap, whilst the extinction spectrum illustrates polarization independence. With broken symmetry, multi-wavelength resonances are observed due to the single dipole resonance and dipole–dipole coupling effect, and wide tunability is also available through minor structural adjustment. Especially when illuminated by a circularly polarized light beam, the extinction and the electric field distribution can be effectively modulated by just varying the incident wavelength.

OCIS codes: 260.5430, 290.2200, 250.5403.
doi: 10.3788/COL201816.052501.

Plasmonic nanoantennas, which usually consist of metallic nanoparticles, figure prominently in many fields, such as plasmonics[1], nonlinear optics[2], biosensing[3], and wireless communications[4]. Owing to the excitation of the localized surface plasmon polaritons (LSPPs), the optical characteristics of these antennas are highly sensitive to the shape and size of the nanoparticles, the optical parameters of the surrounding environment, etc. Thus, by optimal design, these antennas provide an effective way to adjust their electromagnetic responses, i.e., to control the energy transfer between the freely propagating radiation and the LSPPs at the deep nanoscale.

Recently, various plasmonic nanoantennas of different geometries have been explored[5–7], while much effort was focused on the dipole antennas of C_{2v} symmetry[8–12]. The strong localized field in the feed gap of the dipole antennas can easily yield an enhancement of several thousand, resulting in wide potential applications for biosensing, optical trapping[13], Raman scattering[14], and so on. However, the C_{2v} symmetry only allows resonance along the major axis of the dipole antennas in the feed gap, and its extinction property and electric filed enhancement are rather unstable and polarization dependent[15,16]. On the other hand, plasmonic antennas composed of several structured particles are gaining increasing attention. For example, both the symmetric[17] and asymmetric[18] cross antennas have been investigated systematically. Six-particle and eight-particle common-gap plasmonic nanoantennas have been constructed to obtain a broadband spectral response[19]. Metasurfaces formed by arrays of regularly arranged nanoparticles were applied to perform different operations[20]. In this Letter, we investigate a three-arm windmill plasmonic nanoantenna of C_{3v} symmetry[21] in detail with an emphasis on its resonance behavior with and without broken symmetry. It turns out that the extinction characteristics of C_{3v} symmetry are entirely insensitive to the incident polarization. The opposite case occurs for the volume average electric field enhancement and electric field distribution, whilst the dipole resonance of a single arm yields the maximum enhancement. For the asymmetric case, multi-wavelength resonances appear due to the energy coupling between adjacent arms, which is intimately connected with the structure and polarization. Most interestingly, broad adjustability on the resonance characteristics of a specific asymmetric antenna is available by tuning the circularly polarized or elliptically polarized incident light.

As plotted in Fig. 1, the three-arm windmill plasmonic nanoantenna includes three gold ellipsoids separated by a feed circle gap. The incident laser propagates in the negative z direction, and the antenna is assumed to be surrounded by free space. The commercial finite element method (FEM) package (COMSOL Multiphysics 4.3) is utilized to investigate the proposed structure. In our simulations, the maximum mesh sizes in the free space domain and the metallic region were set to be one tenth of λ/n and one fifteenth of $\lambda/|n|$ for higher precision, respectively. From the widely accepted experimental data, the dielectric function of gold is adopted in the simulation[22]. We simulate the scattering cross-section C_{scat}, the absorption cross-section C_{abs}, the extinction cross-section C_{ext}, and the volume average electric field enhancement E_{avg}, which follows[23]

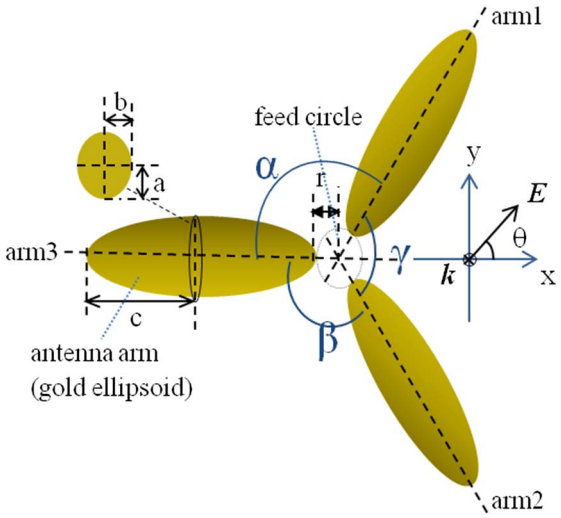

Fig. 1. Schematic of three-arm windmill plasmonic nanoantenna, where the radius of the feed gap is r, the antenna arm is assumed as an ellipsoid with semiaxes $a = b < c$, the angles between adjacent arms are α, β, γ, respectively, and the azimuthal angle between the x axis and the polarization direction is θ.

$$E_{\text{avg}} = \frac{\iiint |\boldsymbol{E}| \cdot \mathrm{d}V}{|\boldsymbol{E}_{\text{inc}}| \cdot V}, \tag{1}$$

where E_{inc} is the incident electric field, and V is the total volume of three gold ellipsoid nanoparticles.

Figures 2(a) and 2(c) show the extinction cross-sections C_{ext} of the symmetrical three-arm nanoantenna and a single gold ellipsoid. It is obvious that the C_{ext} of the nanoantenna is polarization independent, which is different from a single gold ellipsoid. Figures 2(c) and 2(d) can be well explained as follows: the localized surface plasmon resonance (LSPR) along the major axis can be excited when $\theta = 0°$, resulting in the largest C_{ext}. In contrast, the C_{ext} reaches its minimum when $\theta = 90°$, and a weak LSPR can be observed along the minor axis. Based on the statements above, it is not difficult to understand the results of Fig. 2(b), where the resonance strength of each arm relies crucially on the angle between its major axis and the incident polarization. It is interesting to note that what the electric field distribution in Fig. 2(b) does varies for different polarization states, but the C_{ext} of the whole structure remains unchanged. Next, we calculate its volume average electric field enhancement E_{avg} based on Eq. (1), which turns out to be a periodic function. As shown in Fig. 3, E_{avg} is highest when the polarization is parallel to any major axis of its arms, i.e., θ equals 0° or 60° in this simulation. Minimum values of E_{avg} correspond to the case when the polarization is perpendicular to any of the major axes.

Except for the incident polarization, the influence of the geometry parameters, such as the major semiaxis c and the circle gap radius r, are also discussed. From Figs. 4(a) and 4(b) it is clear that both C_{ext} and $\overline{E}_{\text{tip}}$ exhibit a red shift effect as c increases, indicating the strong connection between the surface plasmon polariton (SPP) resonance of the nanoantenna and the LSPR of a single metallic dipole. Figure 4(c) shows a slight blue shift in the resonance wavelength, while the circle gap radius increases from 1.5 to 8 nm, which is in good accordance with the gap-plasmon resonances[24,25]. The peak value of C_{ext} varies very little for different r, but $\overline{E}_{\text{tip}}$ increases drastically since the gap-plasmon resonances are extremely sensitive to the gap size.

In the rest of this paper, we demonstrate that multi-wavelength resonances are the result of the dipole–dipole coupling between adjacent arms if the structural symmetry is broken. First, it should be noted that the asymmetrical structure is no longer polarization independent,

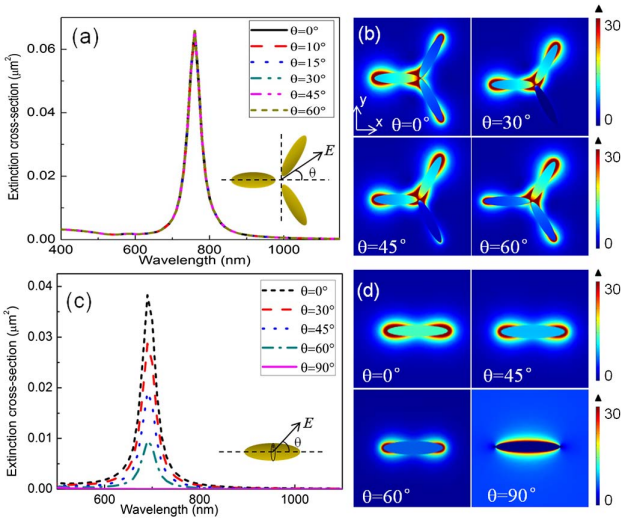

Fig. 2. Comparison of the C_{ext} between the C_{3v} symmetric nanoantenna ($\lambda = 760$ nm) and a single gold ellipsoid ($\lambda = 690$ nm) with different polarization angles. (a) and (b) plot the C_{ext} and the electric field distribution of the nanoantenna, respectively. (c) and (d) plot the C_{ext} and the electric field distribution of the single gold ellipsoid, respectively.

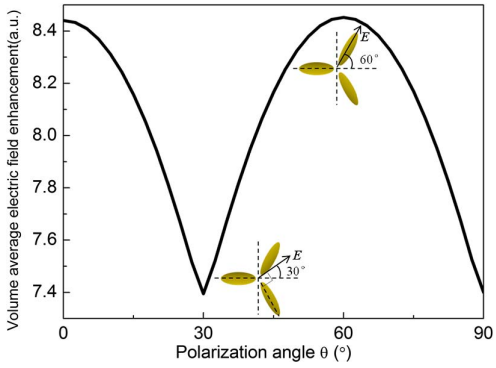

Fig. 3. Dependence of volume average electric field enhancement E_{avg} on the polarization angle θ, where the maximum appears when the polarization direction is along the major axis of an arbitrary arm, and the minimum occurs when they are perpendicular.

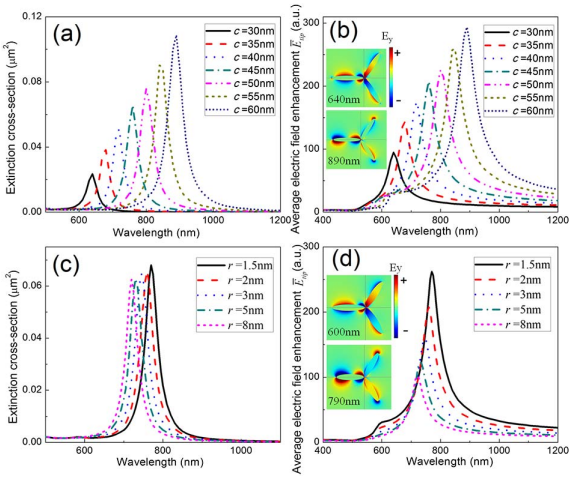

Fig. 4. Variations of (a) the C_{ext} and (b) the average electric field enhancement of three inner tips $\overline{E}_{\text{tip}}$ as a function of the major semiaxis c with $r = 2$ nm. Variations of (c) the C_{ext} and (d) $\overline{E}_{\text{tip}}$ as a function of the gap radius r with $c = 45$ nm. Inset in (b) plots the distribution of E_y at $c = 60$ nm with $\lambda = 640$, 890 nm, respectively. Inset in (d) plots the distribution of E_y at $r = 1.5$ nm with $\lambda = 640$, 890 nm, respectively.

and different polarization states can excite multi-wavelength resonances. For example, we rotate arm2 in the symmetric antenna clockwise for 90° so that $\beta = 30°$. As can be seen from Fig. 5, two linearly polarized beams with $\theta = 0°$ and $\theta = 90°$ share the resonant wavelength at around 736 nm, but they also have an additional resonance each. Not surprisingly, the cross-section C_{ext} corresponds to a circularly polarized light equal to the C_{ext} sum of the two orthogonally polarized beams, so that all resonant peaks are available via adjusting the incident wavelength. For the circular polarization, we plot the electric distribution of the resonant wavelength at 736 and 966 nm, respectively. As plotted in Fig. 5(b), it is different from the state of the C_{3v} symmetric nanoantenna, and the resonance peak at 736 nm is caused by the single dipole resonance of arm1. Also from Fig. 5, we can see that the single dipole resonance is shared by all three different

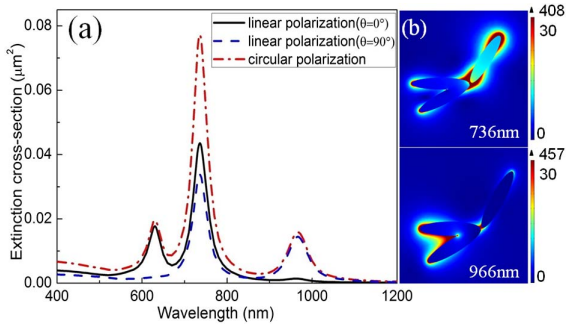

Fig. 5. (a) Extinction cross-section of the symmetry broken plasmonic nanoantenna with $\alpha = 120°$ and $\beta = 30°$ under illumination of linear and circular polarizations; (b) normalized electric field distribution with circularly polarized illumination at resonant wavelengths of 736 and 966 nm, respectively.

polarized states, while the resonance at 966 nm can be attributed to the dipole–dipole coupling effect between arm2 and arm3 due to the vertically polarized state ($\theta = 90°$).

Next, we will prove that resonant wavelength of the dipole–dipole coupling can be modulated if one of the arms can be rotated at will. Numerical simulation was carried out to verify this assumption. In Fig. 6, we rotate arm2 clockwise slightly for 15° to see the variation of the resonant wavelength. It can be found that the peak corresponding to the single dipole resonance displays little shift, since it is contributed mainly by arm1 alone. Since arm2 and arm3 become closer to each other in the rotation process, their dipole resonances tend to couple with each other and splitt. A continuous red shift of the rightmost peak was observed as it varied from 785 to 885 nm, whilst the coupling between arm2 and arm3 is enhanced. So, it is possible that for the dipole–dipole coupling between two adjacent arms, reducing the adjacent angle will result in a red shift of the coupling resonance peak and vice versa. We suggest that this resonance around 640 nm is also resulted from the coupling effect between arm3 and the other two arms, since only linearly polarized light of $\theta = 0°$ is responsible for this resonance. But, this resonance is relatively weak and shows no apparent shift.

The last section is devoted to a rather special asymmetrical structure, where $\alpha = \beta = 90°$; so, arm3 is in the vertical direction of both arm1 and arm2. The results are plotted in Fig. 7(a), where the resonance around 750 nm is shared by linear polarization ($\theta = 90°$) and circular polarization. This resonance is due to dipole resonance along the major axis of both arm1 and arm2, so

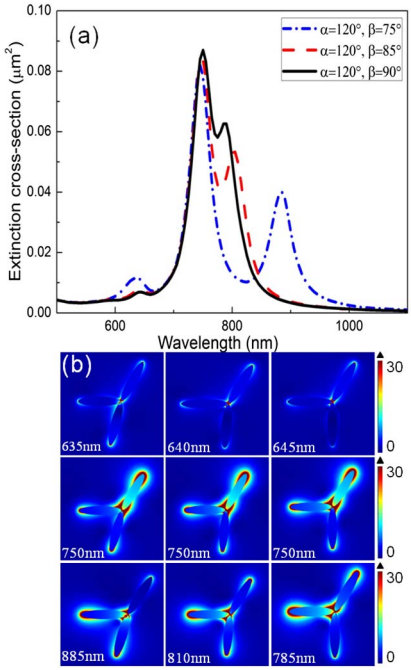

Fig. 6. (a) Splitting and shifting of the resonant peak varying with β at $\alpha = 120°$; (b) normalized electric field distribution at resonant wavelength varying with β.

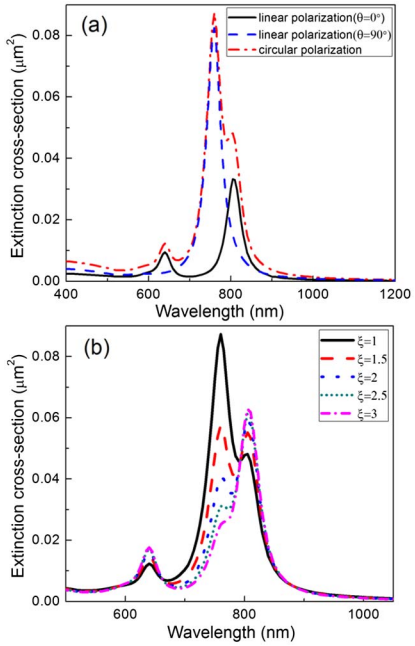

Fig. 7. Extinction cross-section of the symmetry broken three-arm windmill plasmonic nanoantenna for $\alpha = \beta = 90°$ under (a) linearly and circularly, and (b) elliptically polarized incident light.

it is lacking in the case of the linear polarized ($\theta = 0°$) incidence. The dipole resonance of arm3 is coupled with the other two arms and splits into two resonant peaks, which is consistent with the example above. Furthermore, we show that if an elliptically polarized light is applied, the strength of the resonance peaks can also be tailored. For example, we choose the elliptically polarized light as the following:

$$\overrightarrow{E} = \hat{x}\frac{\xi}{\sqrt{\xi^2+1}}\cos(\omega t - kz) + \hat{y}\frac{1}{\sqrt{\xi^2+1}}\sin(\omega t - kz). \quad (2)$$

The relative amplitudes of the extinction spectral peaks are effectively modulated by tuning the parameter ξ in Fig. 7(b), and the physics behind it is obvious. So, for a fixed structure, we can select the resonant wavelength and adjust the resonant strength easily by using elliptical polarization.

In conclusion, this paper has proposed a plasmonic nanoantenna consisting of three identical arms and discussed its resonant behavior for both symmetric and asymmetric arrangements. For the first case, the antenna is found to have a polarization independent scattering cross-section, but its volume average electric field enhancement periodically depends on the polarization angle. For the asymmetrical case, dipole–dipole coupling induced multi-wavelength resonance is observed and can be excited by circularly or elliptically polarized illumination. The resonance can be selected by tuning the incident wavelength, and the resonance strength can also be adjusted through the ellipticity modulation.

This work was supported by the National Natural Science Foundation of China (Grant Nos. 61320106014, 61405117, and 61675104) and the K. C. Wong Magna Fund in Ningbo University, China.

References

1. M. Mesch, B. Metzger, M. Hentschel, and H. Giessen, Nano Lett. **16**, 3155 (2016).
2. L. J. Black, P. R. Wiecha, Y. Wang, V. Paillard, C. Girard, O. L. Muskens, and A. Arbouet, ACS Photon. **2**, 1592 (2015).
3. P. M. Winkler, R. Regmi, V. Flauraud, J. Brugger, H. Rigneault, J. Wenger, and M. F. García-Parajo, ACS Nano. **11**, 7241 (2017).
4. G. Bellanca, G. Calò, A. E. Kaplan, P. Bassi, and V. Petruzzelli, Opt. Express **25**, 16214 (2017).
5. V. Giannini, A. I. Fernández-Domínguez, S. C. Heck, and S. A. Maier, Chem. Rev. **111**, 3888 (2011).
6. X. Zhong, J. Liu, and Z. Li, Chin. Opt. Lett. **12**, 092401 (2014).
7. M. Turkmen, Chin. Opt. Lett. **11**, 070501 (2013).
8. O. L. Muskens, V. Giannini, J. A. Sanchez-Gil, and J. Gomez Rivas, Nano Lett. **7**, 2871 (2007).
9. P. J. Schuck, D. P. Fromm, A. Sundaramurthy, G. S. Kino, and W. E. Moerner, Phys. Rev. Lett. **94**, 017402 (2005).
10. L. Yang, H. Wang, Y. Fang, and Z. Li, ACS Nano **10**, 1580 (2016).
11. W. Yue, Z. Wang, J. Whittaker, F. Lopez-Royo, Y. Yang, and A. V. Zayats, J. Mater. Chem. C **5**, 4075 (2017).
12. H. Jia, F. Yang, Y. Zhong, and H. Liu, Photon. Res. **4**, 293 (2016).
13. W. Zhang, L. Huang, C. Santschi, and O. J. Martin, Nano Lett. **10**, 1006 (2010).
14. W. Zhang, H. Fischer, T. Schmid, R. Zenobi, and O. J. Martin, J. Phys. Chem. C **113**, 14672 (2009).
15. W. Rechberger, A. Hohenau, A. Leitner, J. R. Krenn, B. Lamprecht, and F. R. Aussenegg, Opt. Commun. **220**, 137 (2003).
16. P. Klaer, G. Razinskas, M. Lehr, K. Krewer, F. Schertz, X. F. Wu, and H. J. Elmers, Appl. Phys. Lett. **106**, 261101 (2015).
17. P. Biagioni, J. S. Huang, L. Duò, M. Finazzi, and B. Hecht, Phys. Rev. Lett. **102**, 256801 (2009).
18. P. Biagioni, M. Savoini, J. S. Huang, L. Duò, M. Finazzi, and B. Hecht, Phys. Rev. B **80**, 153409 (2009).
19. E. S. Ünlü, R. U. Tok, and K. Şendur, Opt. Express **19**, 1000 (2011).
20. Y. Hwang and T. J. Davis, Appl. Phys. Lett. **109**, 181101 (2016).
21. D. E. Gómez, Z. Q. Teo, M. Altissimo, T. J. Davis, S. Earl, and A. Roberts, Nano Lett. **13**, 3722 (2013).
22. P. B. Johnson and R. W. Christy, Phys. Rev. B **6**, 4370 (1972).
23. M. W. Knight and N. J. Halas, New J. Phys. **10**, 105006 (2008).
24. L. Guerrini and D. Graham, Chem. Soc. Rev. **41**, 7085 (2012).
25. A. M. Funston, C. Novo, T. J. Davis, and P. Mulvaney, Nano Lett. **9**, 1651 (2009).